Journal of Microscopy

Journal of Microscopy, 2011
Received 6 May 2011, accepted 17 May 2011

doi: 10.1111/j.1365-2818.2011.03518.x

Simple characterisation of a deformable mirror inside a high numerical aperture microscope using phase diversity

D. DÉBARRE, T. VIEILLE & E. BEAUREPAIRE
Laboratory for Optics and Biosciences, Ecole Polytechnique ParisTech, CNRS, and INSERM, Palaiseau, France

Key words. adaptive optics,microscopy,phase retrieval,wavefront control.

Summary

We present a simple and versatile scheme for characterising amplitude and phase modulation by an active element, such as a deformable mirror, in the pupil plane of a high NA microscope. By placing a mirror in the vicinity of the focal plane of the objective and recording images of the reflected focal spot on a camera, we show that reliable measurements of the influence function of the mirror actuators in the pupil plane of the objective can be obtained using an iterative electric field retrieval algorithm. Compared to direct wavefront sensors, the proposed method allows characterisation for a variety of objectives with different NA and pupil sizes without modification of the setup, requires minimal space inside the microscope, and can be used with pulsed sources such as used for multiphoton microscopy. In order to validate our method, we compare our data to the results obtained with a Shack–Hartmann wavefront sensor, and show that comparable precision is achieved.

Introduction

Active aberration correction schemes have been recently shown to significantly improve the performance of optical microscopes. The aim of such schemes is to compensate for the optical aberrations induced by the microscope and the sample by use of an active element such as a deformable mirror (DM) or a spatial light modulator (SLM), to restore diffraction-limited image quality (Booth *et al.*, 2002). Due to recent improvements in the technology of these active elements, aberration correction has received increasing attention over the past few years, in particular in the field of multiphoton microscopy (Marsh *et al.*, 2003; Rueckel *et al.*, 2006; Débarre *et al.*, 2009; Olivier *et al.*, 2009).

Correspondence to: D. Débarre, Laboratory for Optics and Biosciences, Ecole Polytechnique ParisTech, CNRS, and INSERM, 91128 Palaiseau, France. Tel: +33 1 69 33 50 61; fax: +33 1 69 33 50 84; e-mail: delphine.debarre@polytechnique.edu

A critical step in the setup of an efficient aberration correction scheme is the precise control over the electric field at the back aperture of the objective. It is therefore necessary to calibrate the modulation of the electric field induced by the corrective element. This is particularly critical when a DM is used, as the relationship between the voltage applied to the actuators and the wavefront deformation is not initially known. However most of the proposed approaches can be extended to the case where a SLM is used. Indeed, the electric field modulation critically depends on the exact location of the active element within the optical system as well as on the magnification between the former and the objective. As these are not intrinsic properties of the active element, a specific calibration should be used to control the achieved modulation with sufficient precision.

When the active element is incorporated in an existing microscope, it is often impractical and expensive to also incorporate a direct wavefront sensor for calibrating the electric field modulation, in particular when this sensor is not further used for aberration correction as is the case for sensorless approaches (Booth *et al.*, 2002; Marsh *et al.*, 2003; Débarre *et al.*, 2009; Olivier *et al.*, 2009). Here we hence introduce a new scheme to efficiently characterise the electric field modulation in the back aperture of the objective induced by an active element with minimal change in the experimental setup. Similarly to the work of Turaga *et al.* (Turaga & Holy, 2010), it relies on the measurement of the point spread function (PSF) of the setup incorporating the active element, and on the subsequent retrieval of the electric field modulation in the back aperture of the objective. In this paper the PSF refers to the total PSF of the microscope, including the wavefront shaping device. In the following section, we present the method used for measuring the PSF. Section 3 describes the retrieval of the back aperture electric field modulation induced by the active element. In Section 4, we apply the proposed scheme to the calibration of a DM and compare our experimental results with direct measurements from a Shack–Hartmann sensor (SHS). Finally, in Section 5

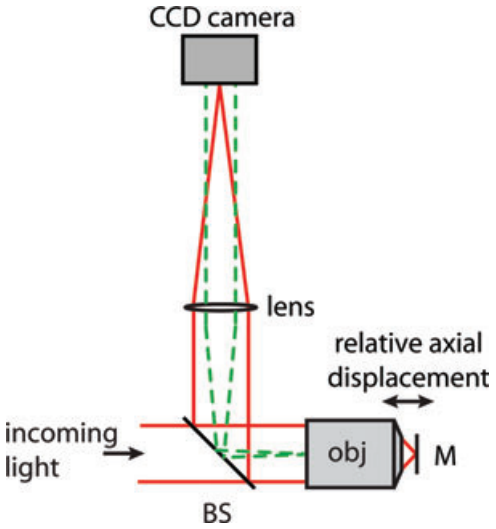

Fig. 1. Typical setup for PSF measurement and subsequent electric field retrieval. BS, plate beamsplitter. Red, light path. Dotted green, pupil and conjugated planes.

we compare our scheme to existing characterisation methods.

PSF measurement

Measurements of the PSF are performed as described in (Botcherby *et al.*, 2008) by use of a mirror M located in the vicinity of the focal plane of the objective and perpendicular to the beam propagation axis (Fig. 1). The reflected light is separated using a 50/50 beamsplitter and focussed onto a charge-coupled device (CCD) camera conjugated with the focal plane. It has been shown (Botcherby *et al.*, 2008) that provided that no aberration is introduced between the focal plane and the CCD plane, an exact magnified image of the PSF at position $2z_0$ from the focal plane is obtained, where z_0 is the axial distance between M and the focal plane. More generally, the measured image can be expressed as the Fourier transform of a modified pupil function:

$$\Pi_{\text{tot}}(\vec{r}) = \Pi_{\text{ill}}(\vec{r})T_o(\vec{r})T_d(-\vec{r})e^{j(\phi_o(\vec{r})+\phi_d(-\vec{r})+\Delta\phi(\vec{r},z_0))}, \quad (1)$$

where Π_{ill} is the illumination pupil function, T_o and ϕ_o (respectively T_d and ϕ_d) are the objective (resp. detection path) amplitude transmission and aberration phase, $\vec{r}$ is the normalised pupil plane coordinate, and $\Delta\phi(\vec{r}, z_0)$ is the defocus term given by

$$\Delta\phi(\vec{r}, z_0) = 2knz_0\sqrt{1-(NA/n)^2r^2}, \quad (2)$$

where k is the wave vector in vacuum, n is the refractive index of the immersion medium and NA is the numerical aperture of the objective. In the general case, T_o and T_d might be different; however in the case pictured on Figure 1, they are equal unless the beam is clipped by the lens. In contrast to equation (1), the microscope PSF can be expressed as the Fourier transform of the pupil function

$$\Pi(\vec{r}) = \Pi_{\text{ill}}(\vec{r})T_o(\vec{r})e^{j(\phi_o(\vec{r})+\Delta\phi(\vec{r},z_0))}. \quad (3)$$

Comparing Eqs (1) and (3) shows that with our method, the phase retrieval algorithm permits reconstructing the modified pupil function $\Pi_{\text{tot}}(\vec{r})$ and not $\Pi(\vec{r})$. However, the two functions only differ by a constant multiplying term $T_d(-\vec{r})e^{j\phi_d(-\vec{r})}$, so that the modulation of the electric field due to the active element can still be measured accurately provided that any zero in the transmission function $T_d(\vec{r})$ coincides with a zero in $T_o(-\vec{r})$. This can be easily ensured provided that the clear aperture of the lens is greater than the objective back aperture, and that no part of the beam is blocked between the mirror and the camera (e.g. by a dust particle).

Electric field retrieval

In a second step, the modified pupil function $\Pi_{\text{tot}}(\vec{r})$ was calculated using a modified Gershberg-Saxton algorithm described in (Hanser *et al.*, 2003) taking into account the large numerical aperture of usual objective lenses. The flow diagram of the algorithm is shown on Figure 2. In brief, the algorithm uses as an input a series of 2D images of the intensity PSF acquired for different positions of mirror M, as described in the previous section. Because the PSF was measured using reflected light rather than fluorescence, raw images exhibited high signal-to-noise ratio, which permitted the use of only three PSF images taken at positions z_0, 0 and $-z_0$, instead of four in the original article (Hanser *et al.*, 2003).

The algorithm ran as follows. The guess for $\Pi_{\text{tot}}(\vec{r})$ at iteration i was used to calculate three 2D amplitude PSFs corresponding to positions z_0, 0 and $-z_0$. These reconstructions were compared to the measured intensity images to estimate the quality of the pupil function guess: if ϵ, the sum of the mean square differences between each reconstructed intensity profile (obtained as the squared absolute value of the reconstructed amplitude PSF) and the corresponding measured profile, normalised to the sum of the mean square values of the three measured intensity profile, was smaller than 0.1%, or if the relative variation of ϵ between iterations $i-1$ and i was smaller than 0.1%, the iterative loop was terminated and $\Pi_{\text{tot}}(\vec{r})$ at iteration i was used to calculate the estimate of the amplitude and phase of the electric field. Otherwise, the phase of the reconstructions were kept while their amplitude were replaced by the measured profiles. After an inverse Fourier transform and removal of the defocus term, the new guess at iteration $i+1$ for $\Pi_{\text{tot}}(\vec{r})$ was calculated by averaging the three estimates for z_0, 0 and $-z_0$ and applying an appropriate constraint on the resulting amplitude (see below for more details). An example of a set of measured 2D PSFs along with the reconstructed amplitude and phase profiles is presented on Figure 3. Phase unwrapping was performed as described in (Booth *et al.*, 2005). The software developed for electric field

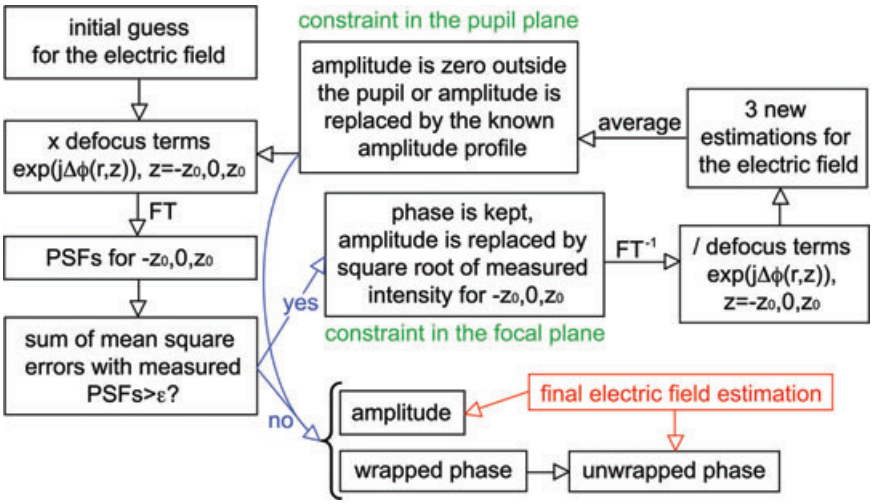

Fig. 2. Flow diagram of the electric field retrieval algorithm. See section 3 for typical values of the different parameters.

retrieval is available for download on our Website (Software for phase retrieval from PSF data available from http://www.lob.polytechnique.fr/home/publications-patents-software/#Software).

To ensure good convergence of the algorithm, the displacement z_0 of the plane mirror between two images should be chosen appropriately. Indeed, as mentioned in (Lofdahl *et al.*, 2000), the PSF exhibits more pronounced changes with aberrations at distances from the focal plane greater than one or more Rayleigh lengths z_R. On the other hand, if z_0/z_R becomes too large, the PSF peak intensity and hence the signal-to-noise ratio drop, which degrades the quality of the retrieved amplitude for the field unless the exposure time is dramatically increased. We found experimentally that choosing $z_0 \approx$

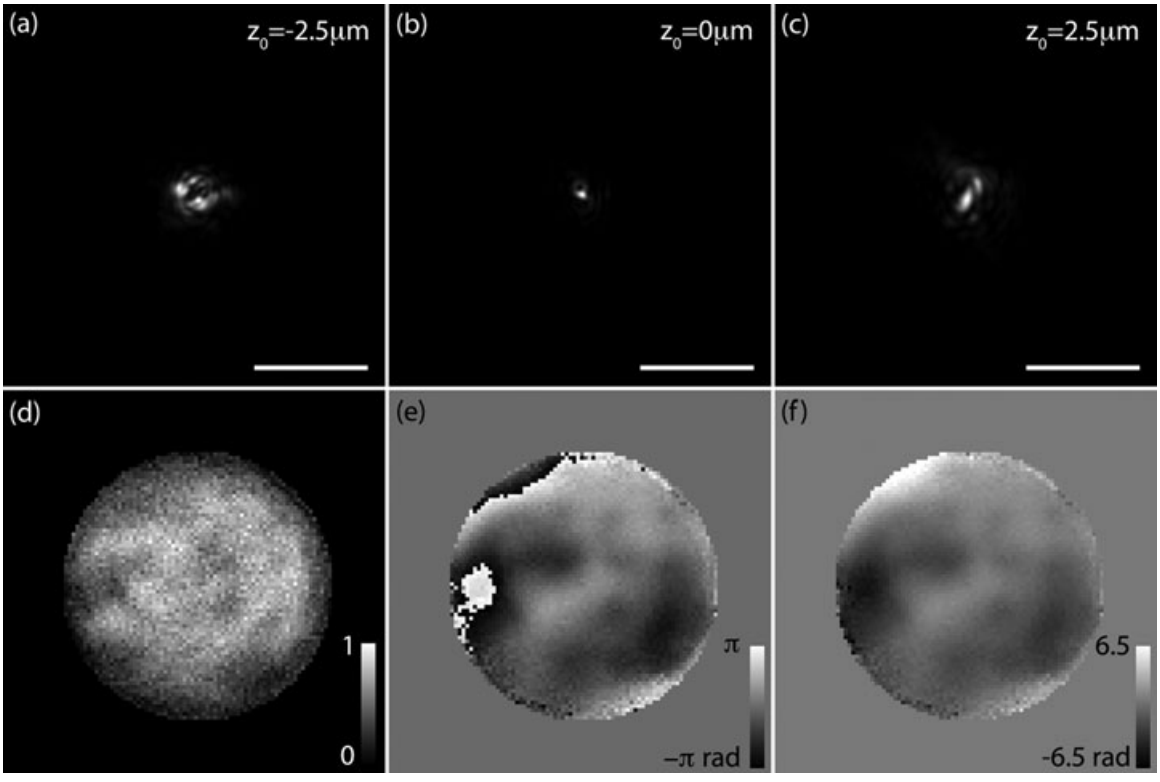

Fig. 3. Example of electric field reconstruction. (a)–(c), 2D PSF images for a 20×, 0.75NA air objective. Scale bar, 10 μm; (d), reconstructed amplitude (arbitrary units); reconstructed phase before (e) and after (f) unwrapping.

2 *to* 5 z_R was a good compromise to ensure convergence of the algorithm without leading to an exceedingly long acquisition time for the data.

The electric field retrieval algorithm can be significantly sped up by using appropriate constraints and initial guesses in the case of the calibration of an active element. Since an upper limit for the objective back aperture diameter can be deduced from its numerical aperture and focal length, the constraint used in the back aperture plane is that the electric field intensity should be zero outside of this boundary. We point out that in the common case where the method is used to calibrate a DM optically conjugated with this plane, a more appropriate constraint can be used: the first retrieval from a given mirror shape is done using the above-mentioned boundary constraint, and the amplitude of the field, which does not depend on the phase applied by the mirror, is kept as a new constraint for the subsequent retrievals (each corresponding to a different applied phase). In addition, the previously retrieved phases can be used to improve the initial phase guess. Using these improved starting conditions, the retrieval process for a pupil diameter of 80 pixels (i.e. 5000 pixels in the back aperture) takes about 30 s for the first retrieval (phase and amplitude) but only about 2 s for each subsequent phase-only retrieval on a 2 GB RAM, 3 GHz computer.

Experimental results

To demonstrate the accuracy of our method, influence functions of actuators of a DM were measured using a test setup shown on Figure 4, incorporating a DM with 52 active elements (MIRAO 52-d, Imagine Optics), a 50/50 beamsplitter plate (CVI Melles Griot), a silver mirror mounted on a piezo stage (PI) and a 1280×960 pixels, 8-bits camera (IDS). Alternatively, a SHS (HASO-3, Imagine Optics) was used for direct electric field measurement and comparison with the phase-retrieval-based calibration. In our experimental setup, the DM was conjugated with the objective back aperture, and the phase retrieval algorithm was used to determine the influence function of each actuator on the phase of the electric field at the back aperture. For each actuator, the influence function was determined by measuring (either through phase retrieval or using direct Shack–Hartmann sensing) the wavefront for several command amplitudes on the actuator. Since our DM is linear, the influence function was obtained by a pixel-by-pixel linear fit of the phase as a function of the command amplitude, after subtraction of the phase value in the centre of the pupil so as to remove the arbitrary phase offset resulting from the retrieval process. This process is straightforwardly extended to the case of a mirror with a non linear relationship between the amplitude of the membrane deformation and the applied command by use of an appropriate fitting function.

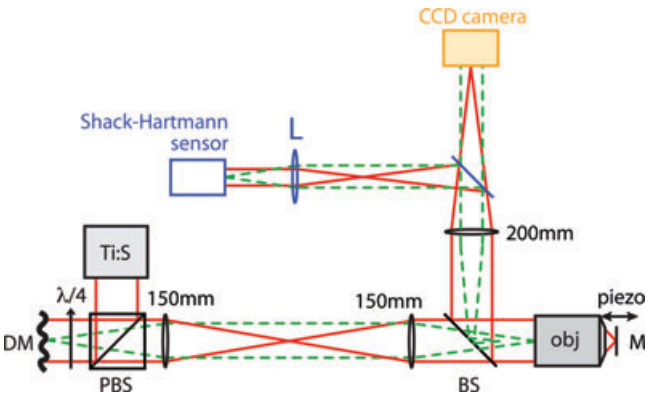

Fig. 4. Experimental setup for calibration of a deformable mirror (DM) for various objective lenses. The lens L was changed for the different objectives so as to adapt the beam size on the Shack-Hartmann Sensor (SHS) used for comparison with the phase-retrieval-based calibration. λ/4, quarter waveplate; PBS, polarizing beamsplitter; BS, 50/50 beamsplitter plate. Light path was switched between the SHS and the CCD by a flip mirror (in blue). Red, light path. Dotted green, pupil and conjugated planes.

Figure 5 shows the influence function for an actuator located near the centre of the pupil of a 60×, 1.2 NA water-immersion objective. The first column shows the electric field retrieval results. The amplitude profile was retrieved for zero voltage applied to the actuator and the phase profile is a fit with 10 different voltages applied. For comparison, the second column shows the direct measurement obtained from the SHS with the same number of voltages applied. The results for the phase are in good agreement with a relative standard deviation $\lesssim$6% as approximately estimated by downsampling the phase retrieval profile to the resolution of the SHS. Although the results are also consistent for the amplitude of the field, with the main features well preserved (e.g. size of the objective pupil), discrepancies exist which arise mainly from the noise in the PSF images (Hanser *et al.*, 2004) and from the positioning errors of the piezo stage. Experimentally, we found that these parameters have noticeable influence on the reconstructed amplitude profile, whereas the reconstructed phase is only marginally affected by positioning errors of up to 30%.

A major advantage of the proposed method is its compactness and versatility when various objectives are used. This is demonstrated on Figure 6 where the influence function of another actuator of the DM was measured for three objectives with very different characteristics : a 10×, 0.25NA air objective with no coverslip correction (LMPlan IR, Olympus, pupil size 9 mm) a 20×, 0.75NA, coverslip corrected air objective (UPlanSApo, Olympus, pupil size 13.5 mm); and a 60×, 1.2NA, coverslip corrected water objective (UPlanSApo UIS2, Olympus, pupil size 5.4 mm). Although these objectives have very different magnifications, numerical apertures and pupil size, the influence function could be retrieved without any change in the setup apart from the objective itself. To accommodate for the difference in pupil sizes, the image from the camera is either cropped (to reduce the number of pixels

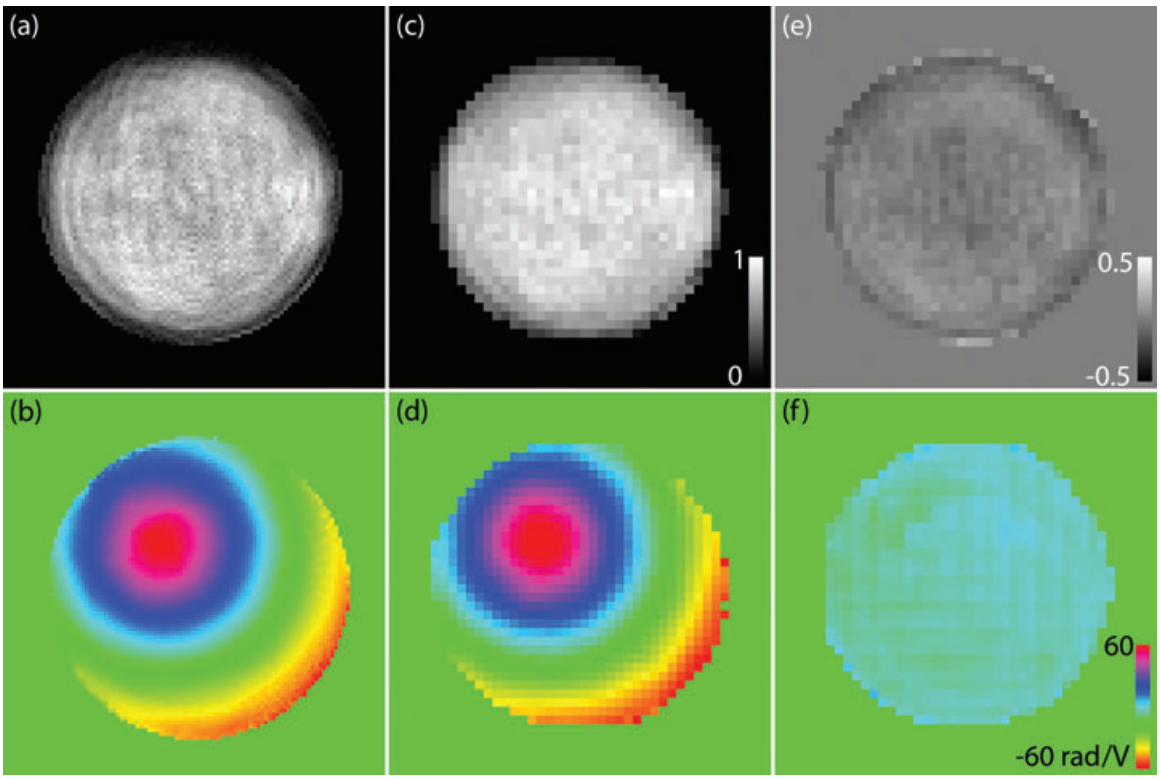

Fig. 5. Amplitude profile of the electric field (top, arbitrary units) and influence function of an actuator of the DM on the phase (bottom) in the pupil plane of a 60×, 1.2NA water-immersion objective. (a,b), electric field retrieval using PSF measurements; (c,d), direct measurement with a SHS. Last column, difference in amplitude (e) and phase (f) between the two methods. Data from the first column have been downsampled to the same resolution as the second column to calculate (e) and (f). The three phase profiles are displayed using the same colour scale.

in the resulting phase profile) or binned (to reduce the size of the margins around the retrieved pupil). Using a 200 mm lens and the above-mentioned 1 Mpixels camera with pixel size 3.75 μm, a resolution of up to 20 000 pixels could be obtained even for the smallest pupil size investigated here (60× objective). This should be compared to the maximum of 800 phase points that can be obtained with optimal filling of our SHS, a value typical for most recent SHSs. As a result for the SHS measurements, we had to change lens L (Fig. 4) depending to the objective lens so as to optimised the filling and permit proper comparison between the two calibrations. The chosen values were 50 mm (20× objective), 100 mm (10× objective) and 150 mm (60× objective).

For the three objectives investigated here, results are in good agreement for the two calibration methods. The main difference can be seen in the first column, where the phase profile obtained from the SHS is clipped in its bottom left part: this was due to the low intensity in this part of the pupil which was as a result automatically clipped by the commercial software of our SHS. This illustrates the good sensitivity and dynamic range of our calibration method.

As a last step, we used the previously measured influence functions to determine the vectors of commands that must be sent to the DM to produce chosen aberration modes, e.g. Zernike modes. To this aim, the influence function of each of the N actuators is decomposed as a sum of M Zernike modes with appropriate coefficients, producing a N-by-M matrix of such coefficients. This matrix is then pseudo-inverted to yield the vectors of commands that produce the best approximation of each of the initial M Zernike modes that the mirror can produce (see Booth *et al.*, 2005, for details).

We measured experimentally the phase variation obtained when applying one of these vectors to the DM. The result for astigmatism is displayed on Figure 7. Both the phase diversity retrieval and the SHS measurement show good agreement with the theoretical corresponding phase profile. Moreover the remaining phase difference between the theoretical and measured profiles, which mainly consists of higher order astigmatism, should not be attributed entirely to imprecisions in the calibration process. A significant part of this difference results from the fact that the mirror cannot produce perfect Zernike modes but rather their projection onto its eigenmodes: indeed, when comparing the measured profile (a) with the phase profile that can be expected from the combination of previously determined influence function of actuators that best fits the chosen Zernike mode, the residual phase (e) is further reduced to a rms value of 0.045 rad.

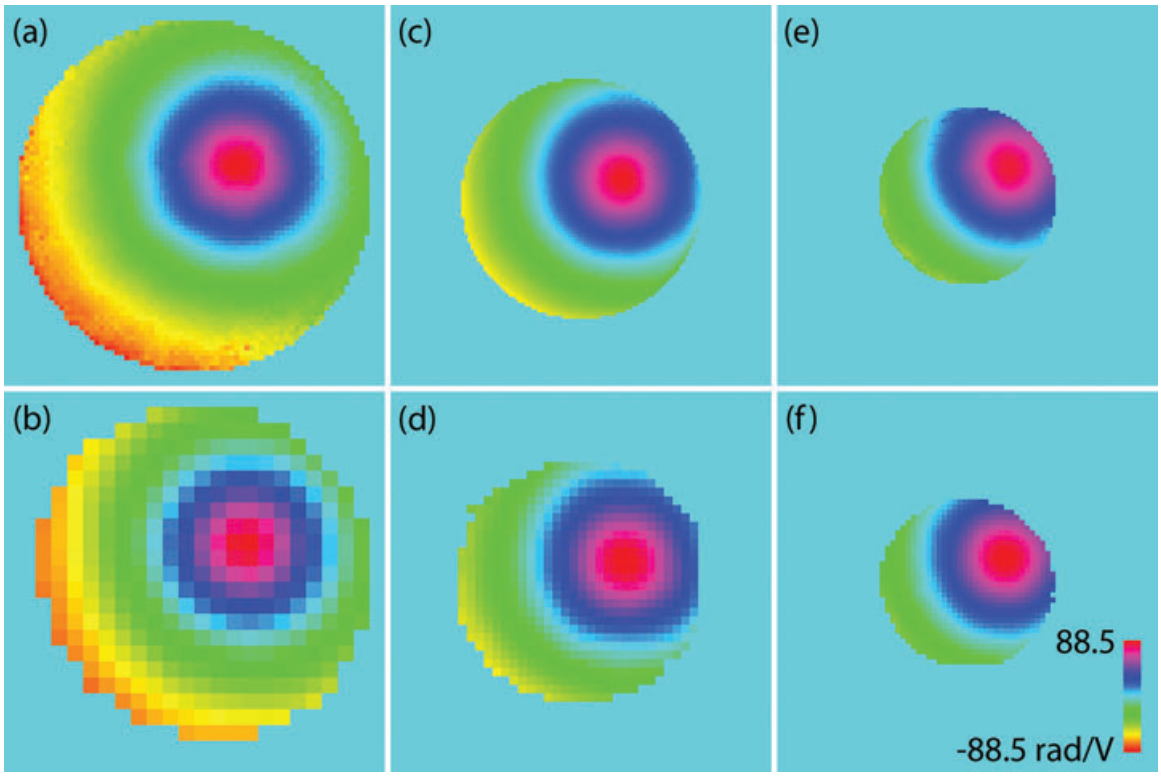

Fig. 6. Influence function of an actuator of the pupil-plane-conjugated DM on the phase in the pupil plane of various objectives, as measured using phase retrieval (top) and a SHS (bottom). First column, 20×, 0.75NA air objective; second column, 10×, 0.25NA air objective; third column, 60×, 1.2NA water-immersion objective. All profiles are displayed using the same colour scale.

Discussion

The method proposed here offers several advantages for calibrating the pupil plane wavefront inside a microscope. As shown in the previous section, it allows for precise determination of the electric field profile with minimal change in the setup of most microscopes. This is consistent with the results of Hanser et al (Hanser *et al.*, 2004) showing in several practical cases the accuracy of their retrieval process. It should also be noted that if the DM is placed in the imaging path instead of the excitation path, the same calibration process can be used with the only difference that the plate beamsplitter will be used this time for injecting the incoming light inside the objective lens.

The use of phase diversity to measure the electric field in the pupil plane of an objective lens has already been proposed in the context of microscopy (Hanser *et al.*, 2003; Turaga & Holy, 2010). Here we introduce a major simplification by measuring the PSF without the use of fluorescence. As a result, measurements are performed more easily and the retrieval algorithm is simpler and yield more accurate results. First, we avoid the need to use a fluorescent object as a light source,

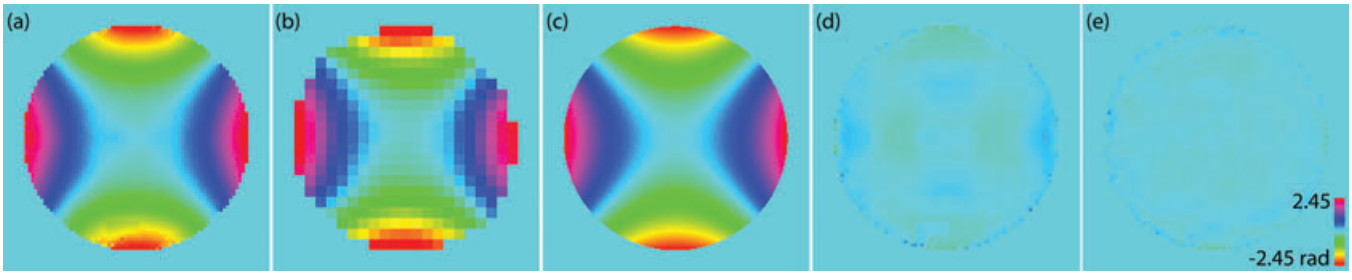

Fig. 7. Phase variation in the pupil plane of the 20×, 0.75NA air objective when the command vector calculated to induce 1 radian rms astigmatism is applied. (a), phase variation retrieved using phase diversity; (b) direct measurement on the SHS; (c), theoretical astigmatism profile; (d), difference between the measured profile (a) and the theoretical profile (c). (e), difference between the measured profile (a) and the profile predicted using the influence functions of the actuators and the vector of commands applied. All graphs share the same colour scale.

thereby avoiding sample preparation and more importantly, convolution of the object shape with the system PSF. Although this effect can be accounted for during the retrieval process (see Hanser *et al.*, 2004), it lowers the signal-to-noise ratio for high spatial frequencies located around the edges of the pupil. This is evidenced by comparing the size of the fluorescent beads typically used for PSF measurements [respectively 0.12 (Hanser *et al.*, 2003; 2004) and 0.2 μm (Turaga & Holy, 2010)] with the beam waist for the higher NA objective investigated here (≈0.4 μm at 800 nm).

Furthermore, our approach provides a higher signal-to-noise ratio without the need for highly sensitive detectors. This allows us to perform electric field retrieval without either filtering the data or making assumptions on the phase and/or amplitude profile. As a comparison, Hanser *et al.* (2003, 2004), when using four images (three in our case), performed phase retrieval after Gaussian smoothing of the measured PSFs, and applied a smoothing filter on the pupil electric field every five iterations. The alternative approach developed by Turaga *et al.* (Turaga & Holy, 2010) uses only one PSF image per actuator position (thereby avoiding the need for a motorised z-positioning system), and performs a global fit of 21 images obtained for different amplitudes for each actuator, thereby mitigating the noise in the images. Convergence was nevertheless obtained by assuming a known amplitude profile in the pupil plane and by modelling the phase deformations induced by the mirror onto a reduced number of functions. One consequence is that the number of independent phase pixels in these cases is smaller than the number of displayed pixels, whereas in the results presented here the number of pixels within the pupil equals the number of independent phase and (unless previous amplitude retrieval data is used) amplitude values.

PSF measurements without the use of fluorescent objects had been proposed by Lofdahl *et al.* (2000) in the context of astronomy. However because in this case the numerical aperture of the imaging lens was very low (≈0.01), direct imaging of the PSF was possible because the size of the waist was several times larger than the size of a camera pixel. This is however not applicable to the case of large numerical aperture optics such as investigated here.

The main disadvantage of the proposed approach relies in the amplitude and phase offset in the optical transfer function introduced by the second pass through the objective and the detection path. Indeed, this prevents in the general case measurement of the phase and transmission profile of the setup in the absence of sample, which could be used to estimate the optical quality of the setup or correct for its static aberrations. As explained in Section 1, this however does not prevent accurate measurement of the modulation of the electric field due to an active element.

An alternative to our method would be to use a direct wavefront sensor to image the pupil plane of the objective after reflection on a mirror located in the focal plane. This method has been previously used in the case of interferometric phase measurement (Débarre *et al.*, 2009; Debarre *et al.*, 2008), and in this paper a SHS has been used for comparison with the electric field retrieval method. Other detectors, e.g. lateral shearing interferometric detectors could also be used.

The main advantage of this alternative is that the calibration of the DM using one of these sensors in a configuration such as described in Figure 4 is much faster than the method proposed in this article. As an example, interferometric calibration of the influence function of one actuator as described in Debarre *et al.* (2008) takes about 20 s with a standard 2GB RAM computer, including image acquisition, when 21 actuator commands are used. Calibration of the DM can thus be performed in a bit more than 15 min. In our setup, image acquisition for 52 actuators and 21 points per actuator took about 3 h, and the subsequent analysis of the data took slightly less than one hour. The acquisition time of the data was mainly limited by the stabilisation time of the mirror M position (about 1s after each displacement) and the low dynamic range of the camera which forced us to sum about 50–200 images to obtain sufficient precision for low intensity features of the PSF. This total time was significantly reduced to about 30 min for the same number of measurements, when using a 14 bits camera (F-125B Stingray, AVT) and the more accurate positioning system of our home-built upright microscope (M-126.D6 motorized stage, PI). The total of 90 min required for calibration is nevertheless longer than what can be obtained with other methods. It should be noted however that this type of calibration usually needs to be performed only once per objective, or only when the optical path between the DM and the objective is changed. Therefore, the additional time needed to install and align the calibration setup should also be taken into account when estimating the time required for calibration. Interferometric measurement, for example, requires that an interferometer be built within the optical path with the DM in one of the arms. When using a wavefront sensing device such as a SHS, careful alignment and conjugation of the device with the back aperture of the objective should be ensured, a procedure more time-consuming than simply placing a camera at the focus of a lens.

In contrast, an advantage of the proposed method over the use of other wavefront sensors to image the pupil plane is the compactness of the setup added for calibration. Indeed, it is easily implemented on most commercial or home-built microscopes : the plate beamsplitter can be inserted in place of the usual dichroic beamsplitters, and the lens and camera only require a total space of about $300 \times 50 \times 50\,\mathrm{mm}^3$. In most cases, standard imaging ports can even be used so that no modification of the microscope is required, offering a cheaper and easier to implement alternative to direct sensors. In addition, the use of a direct wavefront sensor requires that the size of the image of the pupil be adapted to the size of the sensor (CCD camera, SHS, lateral shearing interferometer)

to image the full pupil while keeping a sufficient number of pixels in the resulting pupil profile. This is illustrated by the phase profiles obtained from the SHS in Figures 5–7: with a maximum number of pixels of ≈800 for a circular pupil, the size of the pupil image should be optimised to avoid obtaining a too coarse phase profile, whereas no modification is required for the PSF measurement.

This compactness and versatility makes our method an optimal choice for calibrating a readily built adaptive microscope in which no direct sensor is implemented. Indeed, we point out that the optimal choice for a calibration technique depends on the kind of setup in which the DM is used. As an example, if coherence-gated wavefront sensing is used for aberration correction (Rueckel *et al.*, 2006), interferometric calibration might be best suited as a phase stepping interferometer is already built within the microscope. On the other hand, if closed-loop adaptive optics using a SHS is chosen, such as is usually the case for ophtalmoscopes, the same device can be used for wavefront calibration. Similarly, the method described here is particularly well suited when the DM is then used for wavefront sensorless aberration correction or wavefront shaping (Booth *et al.*, 2002; Marsh *et al.*, 2003; Debarre *et al.*, 2007; Débarre *et al.*, 2009; Olivier *et al.*, 2009), as it offers the cheapest, simplest and most compact set up to fit inside the microscope.

This work was supported by the Agence Nationale de la Recherche (RIB 2007 program).

References

Booth, M., Neil, M., Juskaitis, R. & Wilson, T. (2002) Adaptive aberration correction in a confocal microscope. *Proc. Natl. Acad. Sci. USA* **99**, 5788–5792.

Booth, M., Wilson, T., Sun, H., Ota, T. & Kawata, S. (2005) Methods for the characterization of deformable membrane mirrors. *Appl. Opt.* **44**, 5131–5139.

Botcherby, E., Juskaitis, R., Booth, M. & Wilson, T. (2008) An optical technique for remote focusing in microscopy. *Opt. Commun.* **281**, 880–887.

Debarre, D., Booth, M.J. & Wilson, T. (2007) Image based adaptive optics through optimisation of low spatial frequencies. *Opt. Express* **15**, 8176–8190.

Debarre, D., Botcherby, E.J., Booth, M.J. & Wilson, T. (2008) Adaptive optics for structured illumination microscopy. *Opt. Express* **16**, 9290–9305.

Débarre, D., Botcherby, E.J., Watanabe, T., Srinivas, S., Booth, M.J. & Wilson, T. (2009) Image-based adaptive optics for two-photon microscopy. *Opt. Lett.* **34**, 2495–7.

Hanser, B., Gustafsson, M., Agard, D. & Sedat, J. (2003) Phase retrieval for high-numerical-aperture optical systems. *Opt. Lett.* **28**, 801–803.

Hanser, B., Gustafsson, M., Agard, D. & Sedat, J. (2004) Phase-retrieved pupil functions in wide field fluorescence microscopy. *J. Microsc.* **216**, 32–48.

Lofdahl, M., Scharmer, G. & Wei, W. (2000) Calibration of a deformable mirror and strehl ratio measurements by use of phase diversity. *Appl. Opt.* **39**, 94–103.

Marsh, P., Burns, D. & Girkin, J. (2003) Practical implementation of adaptive optics in multiphoton microscopy. *Opt. Express* **11**, 1123–1130.

Olivier, N., Debarre, D. & Beaurepaire, E. (2009) Dynamic aberration correction for multiharmonic microscopy. *Opt. Lett.* **34**, 3145–3147.

Rueckel, M., Mack-Bucher, J.A. & Denk, W. (2006) Adaptive wavefront correction in two-photon microscopy using coherence-gated wavefront sensing. *P. Natl. Acad. Sci. USA* **103**, 17137–17142.

Turaga, D. & Holy, T.E. (2010) Image-based calibration of a deformable mirror in wide field microscopy. *Appl. Opt.* **49**, 2030–2040.